Optimization of the length and position of the absorber tube in small-scale Linear Fresnel Concentrators

CrossMark

A. Barbón [a], N. Barbón [a], L. Bayón [b, *], J.A. Otero [b]

[a] EPI, Department of Electrical Engineering, University of Oviedo, Gijón, Spain
[b] EPI, Department of Mathematics, University of Oviedo, Gijón, Spain

A B S T R A C T

This paper presents an in-depth analysis of various aspects of small-scale Linear Fresnel Concentrators (LFCs). As we shall see, the influence of the lateral study of the actual absorbed power is very important in this type of LFC. In order to consider the end-effect of the absorber tube, two types of losses need to be taken into account: the end loss and the reflected light loss. Focussing on the optimization of the length and position of the absorber tube, a new mathematical method is presented. The method based on a geometric algorithm allows the straightforward deduction of the optimal design of a small-scale LFC. Numerous numerical simulations are presented for different configurations. This study constitutes the basis of the prototype that is being constructed at a vocational training centre (CIFP-Mantenimiento y Servicios a la Producción) in La Felguera, Asturias, Spain. Asturias, Spain.

© 2016 Elsevier Ltd. All rights reserved.

1. Introduction

Linear Fresnel Concentrators (LFC) are called to play a very important role in future energy sources. LFC present certain advantages in the field of concentrating solar power because of their simplicity, robustness and low capital cost. In Spain, there is already a commercial LFC plant for power generation: Puerto Errado 2 (30 *MW*), in service since August 2012 (see Novatec [1]).

Different LFC configurations have been proposed in the literature (Montes et al. [2]). In the 'conventional' central LFC, there is a single absorber in the centre of the array of mirrors, while in the compact linear Fresnel concentrator (CLFC) (Mills et al. [3]), there is a linear absorber at each side of the mirror array so that consecutive mirrors point to different absorbers. Many possible configurations for the Fresnel receiver model (horizontal, vertical or inclined) have been reported in the literature. Two linear receivers on separate towers with double row tube arrangements of branch tubes are considered in Mills et al. [3]. A multitube Fresnel receiver is presented in Abbas et al. [4], the receiver consisting of a bundle of tubes parallel to the mirror arrays. As to the shape of the mirrors, Abbas et al. [5] analyze the use of different optical designs, including circular-cylindrical and parabolic-cylindrical mirrors with different reference positions. As regards the types of studies

carried out, there are various options: optical design (Montes et al. [2]), economic study (Nixon et al. [6]) and analysis of thermal performance (Singh et al. [7]). LFCs are still much less popular than Parabolic Trough Concentrators (PTC) for concentrated solar applications. An economic comparison of PTCs and LFCs is carried out in Morin et al. [8].

The frontal design of the LFC has been studied by several authors, one of the most well-known methods being 'Mathur's method' (see Mathur et al. [9,10]), which calculates the appropriate value of the shift between adjacent mirrors such that shading and blocking of reflected rays are avoided. However, the lateral design and the lateral optical performance, presented in this paper, has been overlooked until now. A study of this kind may be insignificant in large-scale concentrators, but is a key aspect in small-scale concentrators, more common in the household sector. For example, these concentrators can be used in domestic water heating (Sultana et al. [11]), in the heating/cooling of buildings (Bermejo et al. [12]). It should be borne in mind that this sector represents the largest energy use in Europe, over and above industry, with 26.2% of the total final energy consumption in 2012 (Fetie [13]). In this paper, we consider two separate areas of loss as a result of the lateral study. The first comprises the *inactive part of the tube*, which results in a loss called *end loss*. The second area takes into account the sun's rays that do not fall on the absorber tube, the so-called *reflected light loss*. Some papers actually present partial results, although they are based solely on end loss. The reader can find a brief outline of this type of study in Pu et al. [14]. Elmaanaoui et al. [15] includes

Nomenclature

λ	latitude angle (°)
α_S	height angle of the sun (°)
θ_z	Zenith angle of the sun (°)
γ_S	azimuth of the sun (°)
ω	hour angle (°)
T_S	solar time (h)
Γ	day angle (°)
n_d	ordinal of the day
δ	solar declination (°)
$-\omega_s$	angle of sunrise (°)
ω_s	angle of sunset (°)
θ_t	transversal incidence angle (°)
θ_l	longitudinal incidence angle (°)
Q	total power absorbed (W)
DNI	direct normal irradiance (W/m^2)
$\eta_{opt,0}$	optical efficiency for normal incidence rays (%)
x_{field}	availability of the solar field
CI	cleanliness factor
IAM	incidence angle modifier
IAF	new incidence angle modifier
A_m	total area of the LFC (m^2)
$\eta_{endloss}$	end loss efficiency (%)
$\eta_{optical}$	Optical efficiency (%)
ρ	reflectivity of the primary mirrors
τ	transmissivity of the glass
α	absorptivity of the glass
R	incident radiation, with $|R| = 1$
R_l	longitudinal component of R
R_{ti}	transversal component of R
R_i	resultant of the incident radiation
$R_i{}'$	R_i take into account the incidence cosines
n	number of mirrors at each side of the central mirror
$A_{effective}$	effective area of the absorber tube (m^2)
$L_{endloss}$	length of the inactive part of the tube (m)
f	height of the receiver (m)
L_{abs}	length of the absorber tube (m)
L_u	useful length of the absorber (m)
L_M	length of the mirrors (m)
L_{LRL}	length of loss reflected light (m)
L_a^*	optimal length of the absorber tube (m)
y_i	auxiliary parameters of the lateral design ($i = 1, 2, 3, 4$) (m)
x_i	auxiliary parameters of the lateral design ($i = 1, 2, 3, 4$) (m)
x_0, x_f	auxiliary parameters of the lateral design (m)
β_M	angle between the mirror and the horizontal plane (°)
β_a	angle between the absorber tube and the horizontal plane (°)
μ	angle between the reflected ray and the normal to the NS axis (°)
θ_i	angle between the normal to the mirror and the angle of incidence of the sun (°)
θ_L	lateral incidence angle (°)
l_a^l	left illuminated length of the single absorber tube (m)
l_a^r	right illuminated length of the single absorber tube (m)

a study of end loss efficiency in LFCs in addition to the mathematical equations on which the study was based. The same study is carried out in Muthusivagami [16], but for PTCs.

As for the method used in the simulation of results obtained using the optimal configuration, there are several ray tracing programs. In Mills et al. [3], a raytrace model developed in TRNSYS generates optical collection maps in terms of transverse and longitudinal incidence angles. In Grena et al. [17], a ray-tracing program written in C++ predicts the optical performance of the system. To simulate the scattering and diffraction of light, there exists a well-known software application called TracePro, based on the Monte Carlo ray tracing (MCRT) method (see Xie et al. [18], Lin et al. [19] [20]). The main features of six codes for concentrated solar flux calculation (UHC, DELSOL, HFLCAL, MIRVAL, FIAT LUX and SOLTRACE) are reviewed in Garcia et al. [21]. Nevertheless, in this work we have decided to develop a new code, implemented in Mathematica$^©$, to determine the optimal configuration of the LFC.

The following comprise the main contributions of this paper, all of which are derived from the fact that the study focusses on small-scale LFCs:

-A new modelling of the total power absorbed from the solar field, Q, considering various aspects related to the lateral design. We shall first see how to calculate the variation in the optical performance of a LFC for varying ray incidence angles by means of a more suitable modelling. Second, we shall consider both the end loss and the reflected light loss in the calculation of the effective area of the absorber.
-A new mathematical algorithm that allows the optimization of the position and length of the absorber tube based on the lateral design. The method is based on a geometrical algorithm that minimizes the area between two curves. This study supposes the extension of previous papers, as end loss and reflected light loss are now taken into consideration.

The paper is organized as follows. Section 2 summarizes the main definitions that will be used throughout the paper, both the definitions on which the geometric study (angular relationships) is based and the different parameters that allow us to calculate the power absorbed by the absorber tube of a LFC. In Section 3, we study the influence of the lateral study in Linear Fresnel Concentrators. Section 4 provides a detailed description of the method developed in the paper for optimizing the position and length of the absorber tube based on the lateral design. This new mathematical method is based on an algorithm that minimizes the area between two curves. Several numerical simulations based on the previous method are presented in Section 5 for different configurations of the LFC. Finally, Section 6 summarizes the main contributions and conclusions of the paper.

2. Basic definitions

This section summarizes the main definitions that will be used throughout the paper.

2.1. Angular relationships

A number of programs exist on the market, such as SolPos$^©$ [22], to calculate the sun's position relative to the axis of rotation of the LFC. Let us now see the expressions that allow us to describe the apparent movement of the sun with respect to the LFC (Duffie et al. [23]). The following equation expresses the height angle of the sun

(α_S) as a function of the declination, δ, latitude, λ, and hour angle, ω:

$$\alpha_S = \arcsin[\sin \delta \sin \lambda + \cos \delta \cos \lambda \cos \omega] \quad (1)$$

Spencer [24] provides this approximate expression for the solar declination (δ):

$$\delta = 0.006918 - 0.399912 \cos \Gamma + 0.070257 \sin \Gamma - 0.006758 \cos 2\Gamma + \\ +0.000907 \sin 2\Gamma - 0.002697 \cos 3\Gamma + 0.001480 \sin 3\Gamma \quad (2)$$

where δ is in radians, the *day angle*, Γ, is defined as a function of the day of the year and is calculated (in radians) as:

$$\Gamma = (n_d - 1)\frac{2\pi}{365} \quad (3)$$

and n_d is the ordinal of the day. The zenith angle of the sun, θ_z, is also commonly used, or the complementary angle to the height angle of the sun ($\theta_z = 90° - \alpha_S$). When the altitude $\alpha_S = 0$, the sun is said to rise (Sunrise) or set (Sunset). From Equation (1):

$$\cos(\omega) = -\frac{\sin \delta \sin \lambda}{\cos \delta \cos \lambda} = -\tan \delta \tan \lambda \quad (4)$$

and hence the angle of Sunrise ($-\omega_s$) and of Sunset (ω_s) can be calculated with:

$$\omega_s = \arccos[-\tan \delta \tan \lambda] \quad (5)$$

The following equation allows us to calculate the azimuth angle of the sun, γ_S, for the northern hemisphere, measured from the South:

$$\gamma_S = sign(\omega).\arccos\left[\frac{\sin \alpha_S \sin \lambda - \sin \delta}{\cos \alpha_S \cos \lambda}\right] \quad (6)$$

where the function $sign(\omega)$ enables our sign convention to be fulfilled, as before noon, $\omega < 0$ and $\gamma_S < 0$, while after noon, $\omega > 0$ and $\gamma_S > 0$.

Considering a LFC aligned horizontally and aligned in a North-South orientation, the angle of incidence of solar radiation will be calculated in two projection planes (see Barbon et al. [25]): the transversal incidence angle, θ_t, and the longitudinal incidence angle, θ_l. The former (θ_t) is defined as the angle between the vertical and the projection of the sun vector on the EW plane (the plane orthogonal to the receiver), while θ_l is defined as the angle between the vertical and the projection of the sun vector on the NS plane.

The transversal incidence angle and the longitudinal incidence angle are deduced from Fig. 1:

$$\theta_t = \arctan\left(\frac{\sin \gamma_S}{\tan \alpha_S}\right) \quad (7)$$

From Fig. 1 follows that:

$$\theta_l = \arctan\left(\frac{\cos \gamma_S}{\tan \alpha_S}\right) \quad (8)$$

But in section 4, for the optimal design, we consider the hour angle, ω, to be fixed at the value $\omega = 0$. So $\gamma_S = 0$ and we obtain:

$$\theta_l = \arctan\left(\frac{1}{\tan \alpha_S}\right) \Rightarrow \tan \theta_l = \frac{1}{\tan \alpha_S} \Rightarrow \theta_l = \theta_z \quad (9)$$

Bearing in mind the lateral study of the LFC, not all the sun's rays reflected by the mirrors fall on the absorber tube. Fig. 2 shows this effect, which gives rise to the two 'terms' that decrease the surface area.

The first term corresponds to the part of the tube that is not illuminated, called the inactive part of the tube, which gives rise to losses known as end loss. These losses have already been taken into consideration by some authors (see, for example, Pu et al. [14], Elmaanaoui et al. [15] and Muthusivagami et al. [16]). They can be minimized via the suitable choice of the position of the absorber tube. This will be one of the objectives of the mathematical optimization presented in Section 4. The second term takes into account the sun's rays that do not fall on the absorber tube, known as *reflected light loss*, resulting from the inappropriate length of the absorber tube. This loss is not taken into account in papers on large-scale LFCs. However, when studying small-scale study LFCs, it is as important as the first type of loss. The second objective of the mathematical optimization in Section 4 will be to maximize the useful length of the absorber tube for a certain length of the
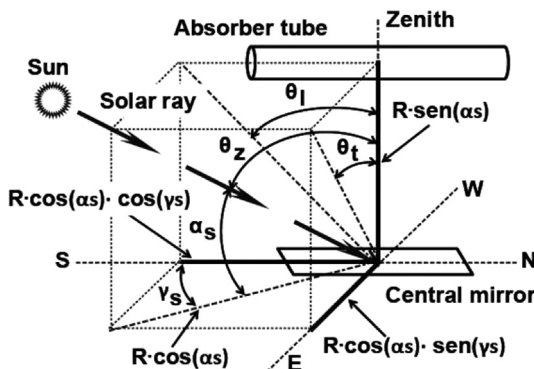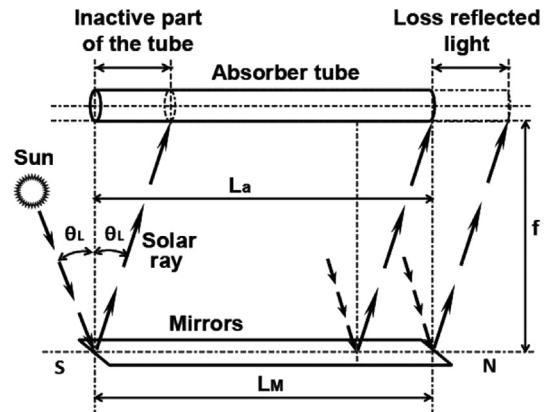

Fig. 1. Basic definitions and angular relationships.

Fig. 2. Lateral study of LFC.

mirrors.

2.2. Power absorbed

Different equations are used in the literature (see, for example, Morin et al. [8], Elmaanaoui et al. [15] and Cau et al. [26]) to determine the power absorbed by the absorber tube of an LFC. All of them are made up of the same terms, in general. The *total power absorbed* from the solar field is thus usually calculated from:

$$Q = DNI \cdot \eta_{opt,0} \cdot x_{field} \cdot CI \cdot IAM \cdot A_m \cdot \eta_{endloss} \tag{10}$$

where the parameters are: *DNI, the direct normal irradiance* (Nikitidou et al. [27]), is the direct irradiance received by a surface that is always held normal to the incoming sun's rays, $\eta_{opt,0}$ is the optical efficiency of the LFC for normal incidence rays to the horizontal ($\theta = 0$) (Nixon et al. [28]), x_{field} is the availability of the solar field; *CI* is the cleanliness factor, *IAM* is the *incidence angle modifier* (Sallaberrya et al. [29]), and describes the variation in optical performances of the LFC for varying rays incidence angles, A_m is the total area of the LFC, and $\eta_{endloss}$ is the *end loss efficiency* (Morin et al. [8]), which describes the amount of the receiver which is not illuminated by the reflected rays.

In this paper, we present a version of this formula which is particularly suitable for the case of working with small-scale LFCs. To do so, we consider the following terms:

$$Q = DNI \cdot \eta_{optical} \cdot IAF \cdot A_{effective} \tag{11}$$

Let us see the meaning of each one of these terms separately.

(i) *DNI* is the direct normal irradiance, defined as usual.
(ii) $\eta_{optical}$ is the total optical yield. Thus, we consider the reflectivity, ρ, of the mirrors, the cleanliness factor both of the mirror, CI_m, and of the glass covering the secondary absorber, CI_g, the transmissivity, τ, of this glass and the absorptivity, α, of the material of which the absorber tube is made:

$$\eta_{optical} = (\rho \cdot CI_m) \cdot (\tau \cdot CI_g \cdot \alpha) \tag{12}$$

Although some of these parameters, especially τ, should change with the angle of incidence (Duffie et al. [23]), they are considered constant for simplicity (see Binotti et al. [30], and Moghumi et al. [31]); their values have been obtained from Duffie et al. [23].

(iii) Like the *IAM*, the *IAF* considers the variation in the optical performance of a LFC for varying ray incidence angles. However, whereas the *IAM* generally only considers the frontal design for the case of a large-scale LFC, here we simultaneously consider the frontal and the lateral design. In small-scale LFCs, the influence of the lateral design is very important, as we shall see in Section 3. Besides, as this factor is different for each mirror, it will henceforth be denoted as IAF_i.

Observing Fig 1 once again, it can be seen that the incident radiation, R, has two components: longitudinal radiation, R_l, common to all the mirrors, and transversal radiation, R_{ti}, which depends on each mirror. Considering $2n + 1$ mirrors (a central mirror and n mirrors on each side of it), they can easily be proved to satisfy the following equalities:

$$R_l = \frac{R \cos \alpha_S \cos \gamma_S}{\cos \alpha_S} = R \cos \gamma_S \tag{13}$$

$$R_{ti} = \frac{R \cos \alpha_S \sin \gamma_S}{\sin \theta_t}; \; 0 \leq i \leq 2n \tag{14}$$

The sum of these two concurrent vectors is:

$$R_i^2 = R_l^2 + R_{ti}^2 + 2R_l R_{ti} \cos \widehat{R_l R_{ti}}; \quad 0 \leq i \leq 2n \tag{15}$$

If we now take into account the terms introduced by the incidence cosines at each mirror, both the lateral term (θ_L) and the frontal term (θ_i), we get:

$$R_l' = R_l \cos \theta_L \tag{16}$$

$$R_{ti}' = R_{ti} \cos \theta_i; \quad 0 \leq i \leq 2n \tag{17}$$

from which, simply assuming that $\cos \widehat{R_l' R_{ti}'}$ is equal at the entry and exit on each mirror, the resultant IAF_i ($0 \leq i \leq 2n$) is:

$$IAF_i = \left[R_l'^2 + R_{ti}'^2 + 2R_l' R_{ti}' \cos \widehat{R_l' R_{ti}'} \right]^{1/2} \tag{18}$$

Remark: As they do not include the lateral study, most authors use the simplified formula:

$$IAF_i \simeq IAM_i = R \cos \theta_i; \quad 0 \leq i \leq 2n \tag{19}$$

In the case of small-scale LFC, however, this simplification leads to important design errors.

(iv) $A_{effective}$ is the effective area of the absorber tube that is actually illuminated. It should be stressed that the effects of shading and blocking have been taken into account in all the calculations. Using Mathur's method [10] for the frontal design of the LFC means that these effects are avoided for the specified operating conditions. In large-scale LFCs, however, the lateral study is ignored due to the negligible influence it has, usually only considering the total area of the LFC, A_m. Some authors who have introduced the lateral study (see Morin et al. [8] and Cau et al. [26]) only analyze the influence of end loss. To do so, they include a term called efficiency loss, $\eta_{endloss}$, which they consider constant for each installation. As already stated, however, there are in fact two losses that must be considered in the lateral study of LFCs. Let us now see this aspect in greater detail. From Fig. 2, the length of the inactive part of the tube is calculated by the following equation:

$$L_{endloss} = f \cdot tan(\theta_L) \tag{20}$$

where f is the height of the absorber tube and θ_L is the lateral incidence angle. The end loss efficiency is calculated by Cau et al. [26] by the following equation:

$$\eta_{endloss} = \frac{L_{abs} - L_{endloss}}{L_{abs}} = \frac{L_u}{L_{abs}} \tag{21}$$

where L_{abs} is the length of the absorber tube and L_u is the useful length of the absorber. Logically, $\eta_{endloss}$ should preferably be as close to 1 as possible.

On the other hand, reflected light loss is a loss that is not usually considered in the mathematical expression normally used to determine the total incident energy on the absorber tube (10). As we can see, however, it comprises a fraction of the energy that leaves the mirrors, but which does not reach the absorber tube. Harnessing this energy would increase the performance of the LFC. To do so, we need to choose the length and position of the absorber

tube correctly. From Fig. 2, the length of loss reflected light, L_{LRL}, is calculated by the following equation:

$$L_{LRL} = f \cdot \tan(\theta_L) \qquad (22)$$

The optimal length of the absorber tube, L_a^*, would be the one fulfilling the following equation:

$$L_a^* = L_{LRL} + L_u \qquad (23)$$

If the length of the absorber tube were L_a^*, the absorber tube would always be illuminated by solar rays. As we shall see below, however, the problem is that this optimal length of the absorber tube varies with the day of year, n_d, with the hour of the day, ω, and with the arrangement of the absorber tube. Hence, the optimization of the length and the position of the absorber tube is fundamental. We accordingly develop an algorithm in Section 4 able to determine L_a^* for the greatest possible number of days of the year and for the greatest number of hours of each day. The algorithm even allows us to optimize winter months versus summer months, or vice versa. Once the LFC has been designed with the aid of our algorithm, the calculation of $A_{effecive}$ will be straightforward and will take into account the two aforementioned losses.

3. Influence of the lateral study in Linear Fresnel Concentrators

In what follows, we shall perform the lateral study of the LFC. In large scale LFCs, this study is not usually performed for two reasons. First, the size of the absorber does not permit any configuration allowing the modification of its position. Second, the influence of the lateral position can be considered irrelevant in % terms with respect to the total length of the absorber. In small-scale LFCs of small size, however, like those analyzed in this paper, this is a fundamental study, as we shall show next. In large-scale LFCs, the mirrors and the absorber tube are not provided with lateral movement and form an angle of 0° with the horizontal plane (configuration C1).

In this study we shall make use of the following parameters: f, L_M and L_{abs} where: f is the height of the receiver, L_M is the length of the mirrors and L_{abs} is the length of the single absorber tube. The results are obtained considering a specific geographic location. In this case, Almeria (Spain), with latitude 36°50′07″ N, longitude 02°24′08″ W and altitude 22 m.

First, we will analyze the influence of f on end loss efficiency. Fig. 3 shows a study of the distribution of the end loss efficiency as a function of the length of the absorber tube (we consider $L_M = L_{abs}$), for $n_d = 172$, corresponding to the Summer solstice. We see that $\eta_{endloss}$ increases with decreasing f. The same applies for the Winter
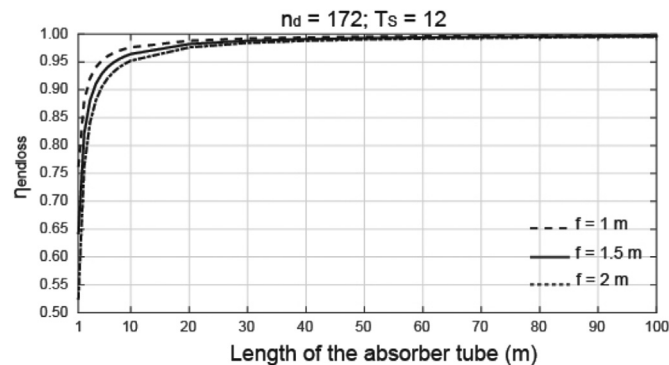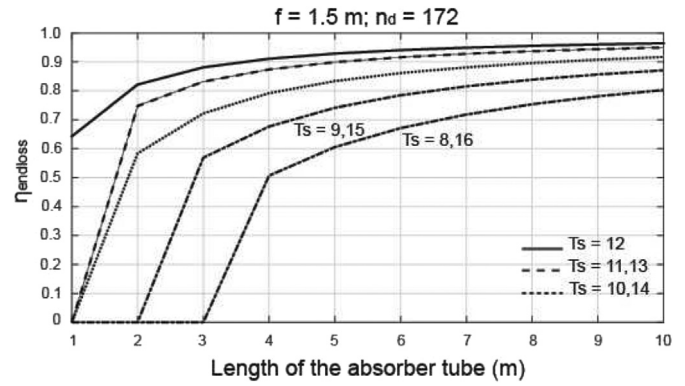
Fig. 4. Influence of T_S. Distribution of the $\eta_{endloss}$ per different L_{abs}.

solstice.

Second, we will analyze the influence of T_S on end loss efficiency, for $f = 1.5$ m and $n_d = 172$. Fig. 4 shows a study of the distribution of the end loss efficiency as a function of the length of the single
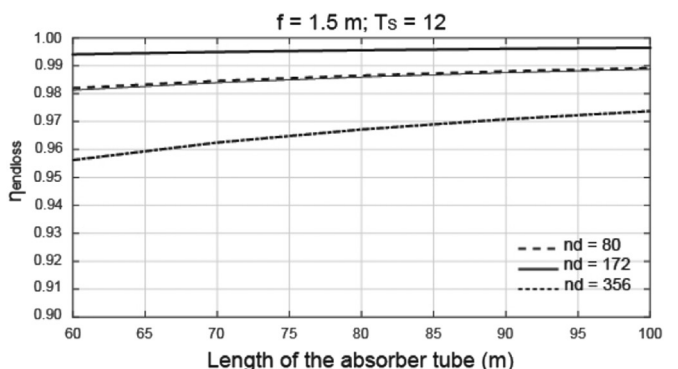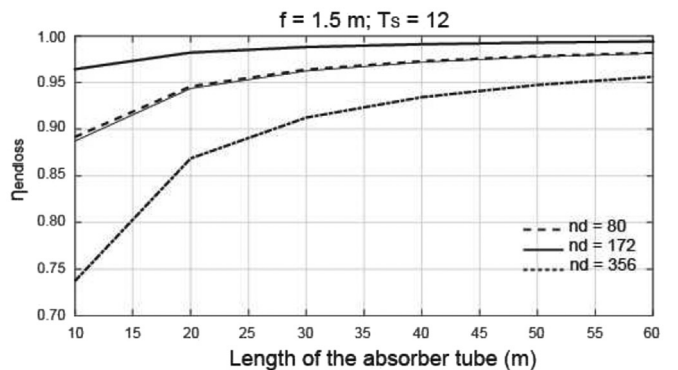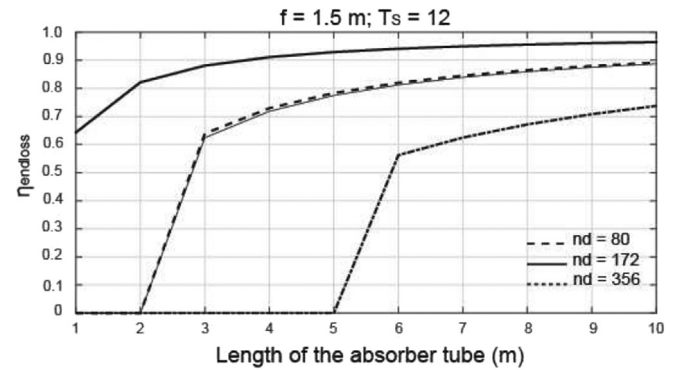
Fig. 3. Influence of f. Distribution of the $\eta_{endloss}$ per different L_{abs}.

Fig. 5. Influence of n_d Distribution of the $\eta_{endloss}$ per different L_{abs}.

absorber tube (we consider $L_M = L_{abs}$), for $T_S = 8, 9, 10, 11, 12, 13, 14, 15$ and 16. We see that $\eta_{endloss}$ is optimal for $T_S = 12$. As the figure shows, for $L_{abs} = 1$, the $\eta_{endloss}$ is 0 for $T_S \neq 12$. For $L_{abs} = 2$ the $\eta_{endloss}$ is 0 for $T_S \leq 9$ (or $T_S \geq 15$). I.e., an increase of L_{abs} produces a decrease (for $T_S \leq 12$) of T_S for which $\eta_{endloss}$ is 0.

Third, we will analyze the influence of n_d on end loss efficiency, for $f = 1.5$ m and $T_S = 12$. Fig. 5 shows a study of the distribution of the end loss efficiency as a function of the length of the absorber tube (we consider $L_M = L_{abs}$), for $n_d = 80$ (Spring equinox), 172 (Summer solstice) and 356 (Winter solstice). We see that $\eta_{endloss}$ is optimal for $n_d = 172$.

Table 1 summarizes the values of L_{abs} and n_d for which $\eta_{endloss} = 0$, for any time of the day.

According to these results, the configuration C1 is not suitable for LFC of low length of the absorber tube.

For $f = 1.0$ m, $n_d = 172$ and $T_S = 12$, the value of $\eta_{endloss}$ is 0.99 for $L_{abs} = 23.82$ m. For $L_{abs} \geq 23.82$ m one gets $\eta_{endloss} \geq 0.99$, for more days and more hours per day. For $f = 1.5$ m, $n_d = 172$ and $T_S = 12$, $\eta_{endloss} = 0.99$ for $L_{abs} = 35.73$ m. For $L_{abs} \geq 35.73$ m one gets $\eta_{endloss} \geq 0.99$, for more days and more hours per day. For $f = 2.0$ m, $n_d = 172$ and $T_S = 12$, one has $\eta_{endloss} = 0.99$ for $L_{abs} = 47.64$ m. For $L_{abs} \geq 47.64$ m one gets $\eta_{endloss} \geq 0.99$, for more days and more hours per day.

Another aspect to consider is the installation of several LFC, connection with the shadows that occur between them. The inclination of the absorber tube and/or the array of mirrors are parameters that influence the classification of the LFC. For $L_{abs} \geq 4$ m, the installation is not possible, for technical reasons. According to these considerations, one has to consider small scale as having L_{abs} less than 3 m.

4. Optimization of the absorber's position and length based on the lateral design

The aim is to compute the optimal relative disposition between the field of primary mirrors and the absorber and the optimal length of the absorber, L_a^*. Fig. 6 represents the general case, such that all the other configurations that we analyze shall constitute particular cases of this one.

Due to lateral symmetry, we only need to take into account the central mirror for this study. In this figure, β_M is the angle between the mirror and the horizontal plane, β_a is the angle between the absorber tube and the horizontal plane, θ_z is the zenithal solar angle, L_M represents the length of the mirrors, f is the distance between the absorber and the mirror, μ is the angle between the reflected beam and the zenith, and θ_L is the angle between the incident ray and the normal plane to the mirror. The following relations between the angles can be verified:

$$y_1 = f + \frac{L_M}{2} \sin \beta_M \tag{24}$$

$$y_2 = \left[x_0 + \frac{L_M}{2} \cos \beta_M \right] \tan \beta_a \tag{25}$$
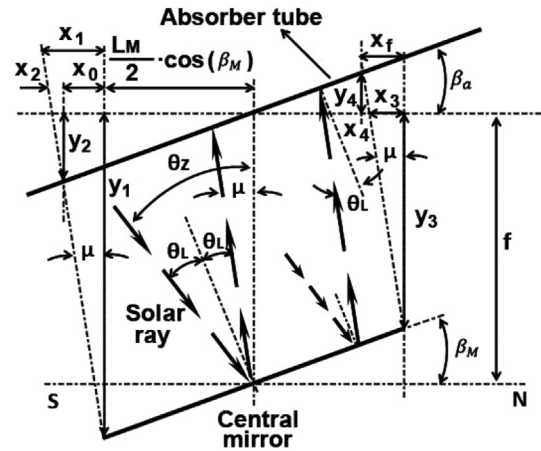

Fig. 6. Definitions used in the lateral design.

$$y_3 = f - \frac{L_M}{2} \sin \beta_M \tag{26}$$

$$y_4 = \left[\frac{L_M}{2} \cos \beta_M - x_f \right] \tan \beta_a \tag{27}$$

$$x_i = y_i \tan \mu; \quad i = 1, 2, 3, 4 \tag{28}$$

$$\mu = 2\beta_M - \theta_z \tag{29}$$

Hence, after some computations, we have that:

$$x_0 = x_1 - x_2 = \frac{\left[f + \frac{L_M}{2} [\sin \beta_M - \cos\beta_M \tan \beta_a] \right] \tan \mu}{1 + \tan \beta_a \tan \mu} \tag{30}$$

and

$$x_f = x_3 + x_4 = \frac{\left[f + \frac{L_M}{2} [\cos \beta_M \tan \beta_a - \sin \beta_M] \right] \tan \mu}{1 + \tan \beta_a \tan \mu} \tag{31}$$

We thus define the left illuminated length of the absorber, l_a^l, as:

$$l_a^l = \frac{x_0 + \frac{L_M}{2} \cos \beta_M}{\cos \beta_a} \tag{32}$$

and the right illuminated length of the absorber, l_a^r, as:

$$l_a^r = \frac{\frac{L_M}{2} \cos \beta_M - x_f}{\cos \beta_a} \tag{33}$$

In the sign convention we have adopted, lengths from the centre of the mirror to the left are considered positive, and those to the right, negative. Thus, when we optimize the values of l_a^l and l_a^r, we calculate not only the optimal length of the absorber tube, L_a^*, but also its position relative to centre of the mirror in the longitudinal direction.

Let us now assume a fixed geographic location for the LFC, which will establish the latitude, λ. The expressions (32) and (33) indicate that both l_a^l and l_a^r are a function of β_M, β_a and μ. In the next section, we shall see that the angles of inclination of the mirrors and the absorber tube, β_M and β_a, will in turn depend on θ_z, δ and λ. Therefore, once λ is fixed and in virtue of the relations (1) and (2), the longitudes (32) and (33) will be a function of two variables: the day of year, n_d, and the hour angle, ω:

Table 1
Values of L_{abs} and n_d for which $\eta_{endloss} = 0$.($f = 1.5$ m)

$L_{abs}(m)$		
1	$1 \leq nd \leq 133$	$213 \leq nd \leq 365$
2	$1 \leq nd \leq 88$	$259 \leq nd \leq 365$
3	$1 \leq nd \leq 59$	$288 \leq nd \leq 365$
4	$1 \leq nd \leq 35$	$312 \leq nd \leq 365$
5	$1 \leq nd \leq 9$	$339 \leq nd \leq 365$

$$l_a^l(n_d, \omega); \quad l_a^r(n_d, \omega) \tag{34}$$

For each configuration of the LFC under consideration, we shall make n_d vary between 1 and 365, while considering the hour angle, ω, to be fixed at the value $\omega = 0$, as this is the value of daily maximum radiation, corresponding to solar noon. We believe that this simplification is perfectly acceptable, as the mid hours of the day are those during which the LFC harnesses the most energy. Thus, having fixed ω, we obtain curves of the form $l_a^l(n_d)$ and $l_a^r(n_d)$, like the one shown in Fig. 7. Fig. 7 shows $l_a^l(n_d)$ and a horizontal straight line of value k_l that represents the ideal position of an absorber tube whose position remains constant during every day of the year. Our algorithm will proceed as follows. We seek the optimal value of k_l (horizontal straight line) such that the area between $l_a^l(n_d)$ and k_l is minimum:

$$\min_{k_l} J^l = \min_{k_l} \int_1^{365} \text{Abs}\left[l_a^l(n_d) - k_l\right] dn_d \tag{35}$$

We operate similarly for the other value, $l_a^r(n_d)$:

$$\min_{k_r} J^r = \min_{k_r} \int_1^{365} \text{Abs}\left[l_a^r(n_d) - k_r\right] dn_d \tag{36}$$

By symmetry, it is straightforward to demonstrate that only in the cases in which $\beta_M = \beta_a$ is it verified that:

$$\min_{k_l} J^l = \min_{k_r} J^r \tag{37}$$

By means of the Interpolation command, the algorithm, which has been programmed in Mathematica 10.0©, calculates the curves $l_a^l(n_d)$ and $l_a^r(n_d)$ from the discretized version obtained for $n_d = 1, \ldots, 365$ in (32) and (33). It then uses the NIntegrate command to calculate the shaded area of the figure. Finally, by scanning the values of k_l and k_r, it is able to calculate the minimum value of (35) and (36). The user can choose the discretization with which the scan is performed between the extreme values $\{\min l_a^l(n_d), \max l_a^l(n_d)\}$ and $\{\min l_a^r(n_d), \max l_a^r(n_d)\}$. In the following section, we shall see the benefits of the algorithm.

5. Numerical simulation

Let us now see the performance of our algorithm for the lateral design of our small-scale LFC. We proceed to show 12 different configurations for the relative position between the field of primary mirrors and the absorber. Table 2 shows and clearly defines the 12 design cases. Of all the configurations, we wish to highlight C_1, which is the configuration used in large-scale LFCs. The mirrors and the absorber tube are not provided with lateral movement and
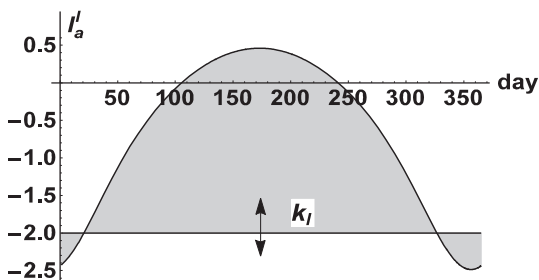
Fig. 7. Illustration of the optimization algorithm.

Table 2
Optimal design for each configuration.

Configuration	Mirrors		Absorber	
	$\beta_M(°)$	Motion	$\beta_a(°)$	Motion
C_1	0	No	0	No
C_2	λ	No	0	No
C_3	λ	No	λ	No
C_4	$\lambda - \delta$	Yes	$\lambda - \delta$	Yes
C_5	$\lambda - \delta$	Yes	λ	No
C_6	$\lambda - \delta$	Yes	$\lambda/2$	No
C_7	$\lambda - \delta$	Yes	21.47	No
C_8	$\lambda - \delta$	Yes	0	No
C_9	$\theta_z/2$	Yes	$\theta_z/2$	Yes
C_{10}	$\theta_z/2$	Yes	λ	No
C_{11}	$\theta_z/2$	Yes	21.47	No
C_{12}	$\theta_z/2$	Yes	0	No

form an angle of 0° with the horizontal plane. This configuration will be used as a basis for the sake of comparison with the other configurations. The C_2 and C_3 configurations lack motion, as the base configuration, C_1. They are used to compare the results with the C_1 configuration in the absence of movement, both of the absorber tube and of the mirrors. Configuration C_2, has an angle of inclination of the mirrors equal to the latitude, with the absorber tube remaining in the horizontal position. In configuration C_2, both mirrors and the absorber tube have an inclination equal to the latitude. The rest of the configurations modify the possibility of movement or the angle of inclination of the mirrors and the absorber.

It is obvious that these configurations that imply inclining the entire mirror row and/or inclining the entire absorber tube seem to work only for small-scale LFC, since it would be unrealistic to incline large-scale LFC. Position C_4 is inspired by a setting similar to that used in the so-called single axis polar solar tracker. These followers rotate on an axis oriented in the NS direction at an axial inclination equal to the latitude of the place, sometimes corrected by means of the declination. Thus, the rotation axis of the system is parallel to the axis of the Earth. Single axis polar solar trackers reach yields of over 96% compared to systems with two axes. Taking this as the base configuration, we make the changes that result in the C_5 to C_8. In the C_9, C_{10}, C_{11} and C_{12} configurations, the rays reflected by the mirrors in the longitudinal direction are always vertical for any time of day, varying the angle of incidence on the absorber tube for each of these configurations. It can be seen that when β_M or β_a depend on δ or θ_z, the mirrors and absorber must be able to move, as these angles vary with the day and time. In configurations C_7 and C_{11} el the absorber tube is not provided with lateral movement and forms an angle of 21,47°. This was chosen as the value of θ_z, corresponding to day $n_d = 195$, which is the day of year with the maximum solar radiation, and to the hour angle, $\omega = 0$ (solar noon).

Fig. 8 shows the results obtained with our algorithm for all 12 configurations. In all cases, the upper curve is $l_a^l(n_d)$ and the lower curve, $l_a^r(n_d)$.

The figure also shows the optimal values of k_l and k_r obtained with our algorithm. The distance between the two values defines the optimal length of the absorber:

$$L_a^* = k_l - k_r \tag{38}$$

Table 3 shows the numerical results for each configuration. These results were obtained by setting $f = 1.5$ (m) and $L_M = 2$ (m). These dimensions are considered optimal for the design of a small-scale LFC and were obtained by applying Mathur's method [9], [10].

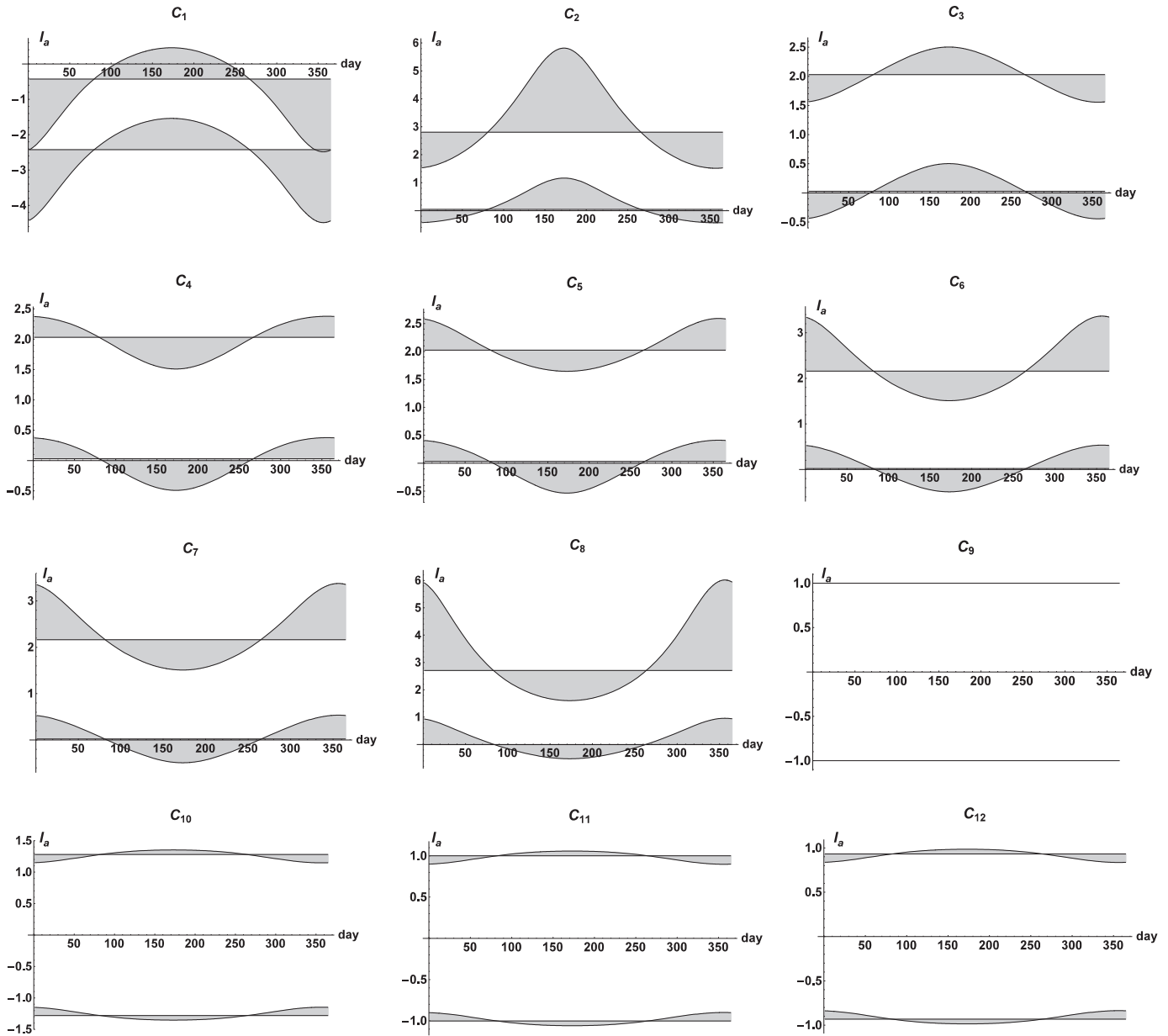It can be seen that the configurations in which the mirrors and

Fig. 8. Optimal design for each configuration.

Table 3
Configurations.

Config.	k_l^*	k_r^*	L_a^*	$\min J^l$	$\min J^r$	Energy (MWh)
C_1	−0.42484	−2.42484	2.00	306.93	306.93	5.356
C_2	2.80709	0.04674	2.76	457.30	170.35	4.913
C_3	2.02897	0.02897	2.00	106.34	106.34	4.431
C_4	2.03037	0.03037	2.00	101.03	101.03	3.825
C_5	2.02362	0.03305	1.99	105.75	106.94	4.012
C_6	2.15992	0.02198	2.13	203.54	115.37	3.804
C_7	2.16351	0.02284	2.14	204.66	115.54	3.904
C_8	2.70750	−0.00454	2.71	454.52	158.82	4.394
C_9	1.00000	−1.00000	2.00	0.00	0.00	5.401
C_{10}	1.28136	−1.28136	2.56	23.47	23.47	6.159
C_{11}	1.00215	−1.00215	2.00	18.35	18.35	5.201
C_{12}	0.93261	−0.93261	1.86	17.08	17.08	4.954

the absorber tube are parallel (C_1, C_3, C_4 and C_9) present an optimal absorber length $L_a^* = 2.00$ (m), equal to $L_M = 2.00$ (m), although the

relative position between the absorber tube and mirrors varies in each of these configurations. In configurations C_9, C_{10}, C_{11} and C_{12}, $\beta_M = \theta_z/2$ and they have been designed such that:

$$\mu = 2\beta_M - \theta_z = 0 \tag{39}$$

We thus achieve a very noteworthy effect, as the absorber tube is located on the vertical with respect to the mirrors, thus achieving a more compact design. Table 3 also gives the values of the areas $\min J^l$ and $\min J^r$, which, when measuring the error between the actual curves and the ideal position of the absorber tube, give an idea us of the error made in each configuration.

The last column in Table 3 shows the annual energy absorbed in each configuration. The importance of this study is evident, as the position of the absorber tube modifies the amount of absorbed energy. Within the configurations that do not include movement (C_1, C_2 and C_3), configuration C_1 provides the best results. In this configuration, the centre of the absorber tube is offset to the right of
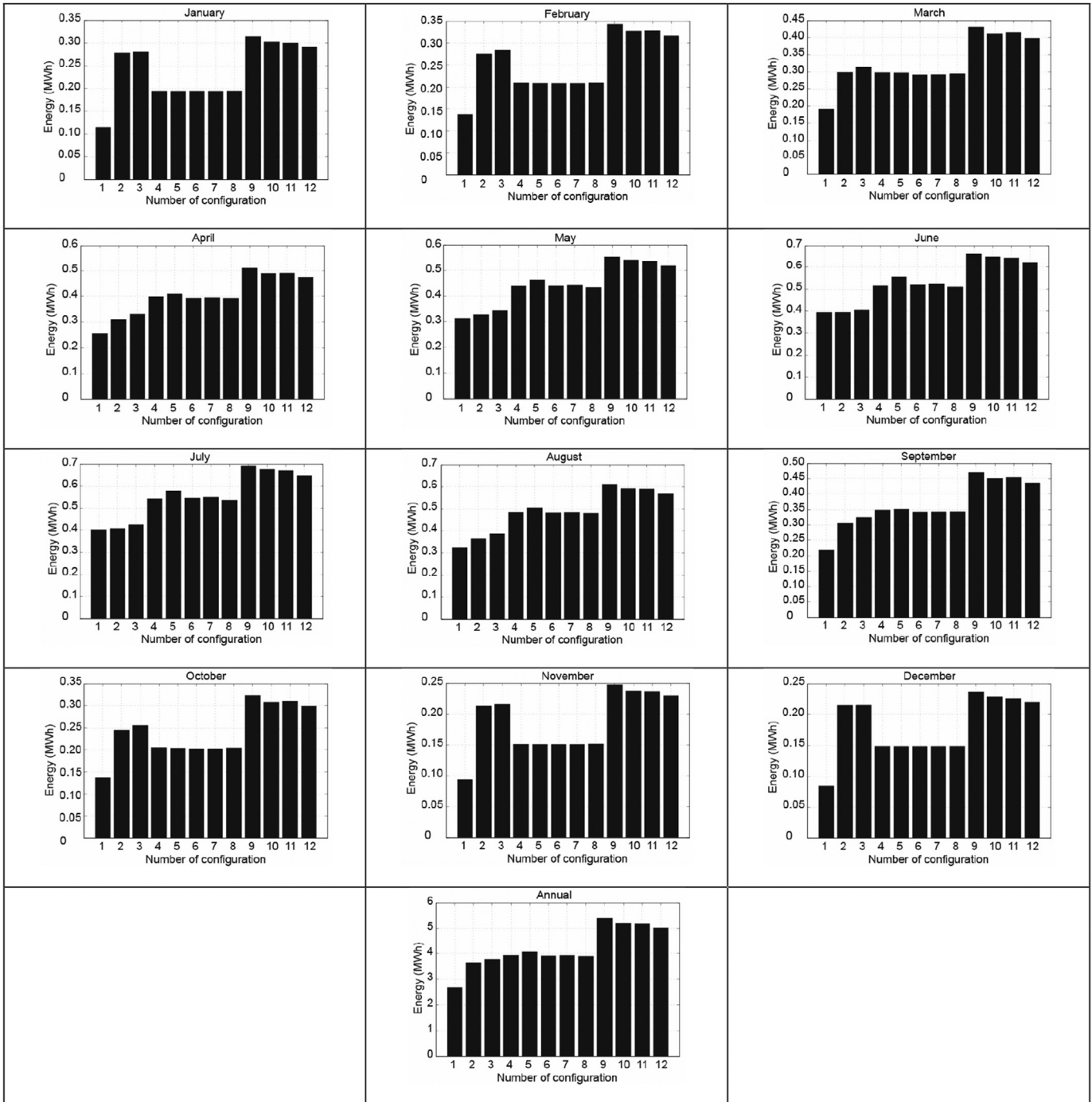
Fig. 9. Energy absorbed.

the longitudinal centre of the mirror. Within the configurations that include movement of the mirrors and the absorber tube (C_4 and C_9), configuration C_9 offers the best results. The configuration that provides the best results for the same length of absorber tube is C_9. These results are very important, as they facilitate the choice of the most suitable configuration.

Fig. 9 shows a study of the distribution of the energy absorbed by the absorber tube per month. The following build parameters were considered in this study: length of mirrors, width of mirror, number of mirrors, focal height, secondary reflector design, diameter of the absorber tube, $L_a^* = 2$ (m), $l_a^l = 1$ (m) and $l_a^r = 1$ (m) (these values were used because they are the same as those of

configuration C_9).

Configuration C_1 presents the best results in the summer months. Configurations C_2 and C_3 present the best results in the winter months. Configurations C_4, C_5, C_6 and C_7 present similar results to one another in the autumn, winter and spring months, and slightly different results in the summer months. Configurations C_9, C_{10}, C_{11} and C_{12} present the best results in the summer months, particularly C_9.

6. Conclusions

Small-scale LFCs are devices with special characteristics that

require a very precise design. Noteworthy among these characteristics is the importance of the lateral study. For that reason, we have presented a mathematical algorithm that enables the absorber's position and length to be optimized based on the lateral design. Note that this concept has not been considered in such detail by any author until now. The results highlight the importance of the location of the absorber tube with respect to the longitudinal centre of the primary reflector, as shown in Fig. 9. In this figure, it can be seen that very different results are obtained depending on the configuration when maintaining a series of build parameters constant. This is an on-going project. These results are currently being used to design a small-scale LFC prototype.

Acknowledgments

References

[1] Novatec-solar, Technical Data NOVA-1, Puerto Errado, 2015. www.novatec-biosol.com/.
[2] M.J. Montes, C. Rubbia, R. Abbas, J.M. Martínez-Val, A comparative analysis of configurations of linear Fresnel collectors for concentrating solar power, Energy 73 (2014) 192—203.
[3] D. Mills, G.L. Morrison, Compact linear Fresnel reflector solar thermal powerplants, Sol. Energy 68 (3) (2000) 263—283.
[4] R. Abbas, J. Muñoz, J.M. Martínez-Val, Steady-state thermal analysis of an innovative receiver for linear Fresnel reflectors, Appl. Energy 92 (2012) 503—515.
[5] R. Abbas, M.J. Montes, M. Piera, J.M. Martínez-Val, Solar radiation concentration features in linear Fresnel reflector arrays, Energy Convers. Manag. 54 (2012) 133—144.
[6] J.D. Nixon, P.A. Davies, Cost-exergy optimization of linear Fresnel reflectors, Sol. Energy 86 (2012) 147—156.
[7] P.L. Singh, R.M. Sarviya, J.L. Bhagoria, Thermal performance of linear Fresnel reflecting solar concentrator with trapezoidal cavity absorbers, Appl. Energy 87 (2010) 541—550.
[8] G. Morin, J. Dersch, W. Platzer, M. Eck, A. Häberle, Comparison of linear Fresnel and parabolic trough collector power plants, Sol. Energy 86 (2012) 1—12.
[9] S.S. Mathur, T.C. Kandpal, B.S. Negi, Optical design and concentration characteristics of linear Fresnel reflector solar concentrators-I. Mirror elements of varying width, Energy Convers. manage. 31 (3) (1991) 205—219.
[10] S.S. Mathur, T.C. Kandpal, B.S. Negi, Optical design and concentration characteristics of linear Fresnel reflector solar concentrators-II. Mirror elements of equal width, Energy Convers. manage. 31 (3) (1991) 221—232.
[11] T. Sultana, G.L. Morrison, G. Rosengarten, Thermal performance of a novel rooftop solar micro-concentrating collector, Sol. Energy 86 (2012) 1992—2000.
[12] P. Bermejo, F.J. Pino, F. Rosa, Solar absorption cooling plant in Seville, Sol. Energy 84 (2010) 1503—1512.
[13] C. Fetie, Statistics on Energy Consumption in Households, EUROSTAT, Vienna, November 2014, pp. 11—12.
[14] S. Pu, C. Xia, End-effect of linear Fresnel collectors, in: Proc. Conf. APPEEC, 2011, pp. 1—4.
[15] Y. Elmaanaoui, D. Saifaoui, Parametric analysis of end loss efficiency in linear Fresnel reflector, in: Renewable and Sustainable Energy Conference, 2014, pp. 104—107.
[16] R.M. Muthusivagami, The impact of end effects in parabolic trough collector pilot set-ups, in: Electrical Energy Systems (ICEES), 2011, pp. 237—239.
[17] R. Grena, P. Tarquini, Solar linear Fresnel collector using molten nitrates as heat transfer fluid, Energy 36 (2011) 1048—1056.
[18] W.T. Xie, Y.J. Dai, R.Z. Wang, Numerical and experimental analysis of a point focus solar collector using high concentration imaging PMMA Fresnel lens, Energy Convers. manage. 52 (2011) 2417—2426.
[19] M. Lin, K. Sumathy, Y.J. Dai, R.Z. Wang, Y. Chen, Experimental and theoretical analysis on a linear Fresnel reflector solar collector prototype with V-shaped cavity receiver, Appl. Therm. Eng. 51 (1) (2013) 963—972.
[20] M. Lin, K. Sumathy, Y.J. Dai, X.K. Zhao, Performance investigation on a linear Fresnel lens solar collector using cavity receiver, Sol. Energy 107 (2014) 50—62.
[21] P. Garcia, A. Ferriere, J.J. Bezian, Codes for solar flux calculation dedicated to central receiver system applications: a comparative review, Sol. Energy 82 (3) (2008) 189—197.
[22] Sun Positions Algorithm Solpos, 2015. http://rredc.nrel.gov/solar/codesandalgorithms/.
[23] J.A. Duffie, W.A. Beckman, Solar Engineering of Thermal Processes, third ed., John Wiley & Sons, New York, 2006.
[24] J.W. Spencer, Fourier series representation of the position of the sun, Search 2 (5) (1971) 172.
[25] A. Barbón, N. Barbón, L. Bayón, J.A. Otero, Theoretical elements for the design of a small scale linear Fresnel concentrator: frontal and lateral views, Sol. Energy 132 (2016) 188—202.
[26] G. Cau, D. Cocco, Comparison of medium-size concentrating solar power plants based on parabolic trough and linear Fresnel collectors, Energy Procedia. 45 (2014) 101—110.
[27] E. Nikitidou, A. Kazantzidis, V. Salamalikis, The aerosol effect on direct normal irradiance in Europe under clear skies, Renew. Energy 68 (2014) 475—484.
[28] J.D. Nixon, P.K. Dey, P.A. Davies, Design of a novel solar thermal collector using a multi-criteria decision-making methodology, J. Clean. Prod. 59 (2013) 150—159.
[29] F. Sallaberrya, R. Pujol-Nadal, V. Martinez-Moll, J.L. Torres, Optical and thermal characterization procedure for a variable geometry concentrator: a standard approach, Renew. Energy 68 (2014) 842—852.
[30] M. Binotti, G. Manzolini, G. Zhu, An alternative methodology to treat solar radiation data for the optical efficiency estimate of different types of collectors, Sol. Energy 110 (2014) 807—817.
[31] M.A. Moghimi, K.J. Craig, J.P. Meyer, A novel computational approach to combine the optical and thermal modelling of Linear Fresnel Collectors using the finite volume method, Sol. Energy 116 (2015) 407—427.